Cite this: *Soft Matter*, 2011, **7**, 3366

www.rsc.org/softmatter

PAPER

Colloidosomes constructed by the seamless connection of nanoparticles: a mobile and recyclable strategy to intelligent capsules†

Conghui Yuan,[a] Yiting Xu,[a] Nina Jiang,[a] Guangjian Chen,[a] Binbin Xu,[b] Ning He[§c] and Lizong Dai*[a]

Received 8th October 2010, Accepted 10th January 2011
DOI: 10.1039/c0sm01128b

Colloidosomes constructed by the self-assembly of nanoparticles (NPs) on liquid–liquid interfaces have been demonstrated to be useful in many fields. However, the interspaces between NPs on the surface of colloidosomes barricade their application in small molecule encapsulation. Herein, fabrication of a new type of colloidosome built by the seamless connection of NPs *via* simply heating and quenching a type of core–shell structured NPs (CSNPs) aqueous system using oil as a template, is presented. These colloidosomes have a hollow structure and exhibit efficient small molecule encapsulation. More importantly, the colloidosomes can dissociate into single NPs and release the small target molecules encapsulated in interior of the colloidosomes at a temperature higher than the melting point of the CSNP shell. It is also shown that the dissociation temperature of colloidosomes can be controlled by simply adjusting the length of the PEG chains in the CSNP shell, which implies that these intelligent capsules have attractive application prospects in controlled drug release.

1. Introduction

The self-assembly of nanoparticles (NPs) has attracted increasing interest in materials science and engineering.[1,2] Such behavior always results in two/three-dimensional ordered structures which are named colloidal crystal arrays. For their potential applications in the optical field,[3–13] macroporous materials,[14–17] separation technology,[18] lithography[19–22] and solar cells,[23,24] several approaches such as gravity sedimentation,[25,26] solvent evaporation,[27–30] physical confinement,[31,32] membrane filtration,[33] template directed synthesis [34–39] and the LB method[40] have been developed to prepare colloidal crystal arrays. These colloidal crystal arrays are identified by their highly ordered structures and low-cost production. However, the NPs are mechanically stacked together in these ordered structures. The inter-particle interaction is weak, transport and environmental change result in the easy dissociation of colloidal crystal arrays.

Recently "colloidosomes", a new morphology self-assembled by NPs on liquid–liquid interfaces, have gained intensive attention.[41] As the NPs are absorbed on the interfaces of two liquids, a heterogeneous reaction can take place on the exposed surface of the particles and heterodimers of two distinct particles can also be produced simply and precisely.[42–50] For their controllable compositions, easy functionalization on specific parts, and tunable particle size, permeability, mechanical strength and compatibility, colloidosomes exhibit applications in controlled drug release,[41] emulsion and foam stabilization[51–55] and fabrication of functional materials.[50,56] The driving force of the adsorption of particles at fluid interfaces is the free energy gained by losing an area of interface. It has been demonstrated that three parameters including the properties of the particle surface, the nature of the liquid–liquid interface and the effective radius of the particles can be used to control the exact location of the NPs on the colloidosome.[2,57,58] For an oil–water system, the contact angle (θ) of NPs measured through the water phase decides the morphology of the colloidosomes. Relatively hydrophilic particles ($\theta < 90°$) preferably form oil-in-water colloidosomes, while relatively hydrophobic particles ($\theta > 90°$) are suitable for stabilizing water-in-oil colloidosomes.[2,55]

Despite its important theoretical value and promising application potentials, this useful and versatile method remains less explored. For example, researchers have realized the control of pore size and permeability. These advantages endow colloidosomes with intelligent encapsulation and controllable release of targeting nanoparticles.[41] However, to control permeability at the scale of macromolecules or even small molecules, further and complicated modifications should be carried out. On the other hand, the particles are normally weakly locked together by electrostatic interactions and van der Waals forces. A stronger locking has been realized by lightly sintering the particles.

[a]*Department of Materials Science and Engineering, College of Materials, Xiamen University, Xiamen, China. E-mail: lzdai@xmu.edu.cn; Fax: +86-592-2183937; Tel: +86-592-2186178*
[b]*Center of Instrumental Analysis, College of Chemistry and Chemical Engineering, Xiamen University, Xiamen, China*
[c]*Department of Chemical and Biochemical Engineering, College of Chemistry and Chemical Engineering, Xiamen University, Xiamen, China. E-mail: hening@xmu.edu.cn; Fax: +86-592-2184822; Tel: +86-592-2183088*

† Electronic supplementary information (ESI) available: Synthetic details of O–B-EGs; ^{1}H NMR spectra, DSC curves, TEM images, SEM images of the resultant products; fluorescence emission spectra of pyrene encapsulated in colloidosomes. See DOI: 10.1039/c0sm01128b

Nevertheless, sintering the particles always requires a relatively high temperature (higher than the boiling point of normal solvents). This disadvantage barricades the use of the sintering method in aqueous solution.

Here we introduce a new type of colloidosomes formed *via* tightly bound monodisperse core–shell structured NPs (CSNPs). These CSNPs are composed of polystyrene (PSt) or poly(methyl methacrylate) (PMMA) cores and amphiphilic polymeric shells with a low melting point (lower than the boiling point of normal solvents). For an oil-in-water system, these CSNPs can be absorbed on the oil droplets to form colloidosomes. The CSNPs on the surface of colloidosomes can reversibly lock together and dissociate by quenching and heating this system, respectively. Moreover, CSNPs are bound so compactly that no interstice exists between the CSNPs. This unique structure allows the colloidosomes to encapsulate and release small molecular drugs.

2. Materials and methods

2.1 Materials

O–B-EG600, O–B-EG1500 and O–B-EG2000 were synthesized by our research group[59] (see ESI†). Styrene and divinylbenzene were purchased from Aldrich. Azoisobutyronitrile (AIBN) was supplied by Alfa Aesar and recrystallized from methanol before use. Pyrene, benzene, ethyleneglycol diacrylate and methyl methacrylate (MMA) were analytical grade and used as received from Shanghai Chemical Reagent Industry.

2.2 Synthesis

P(St-co-O–B-EG600) CSNPs: 0.8 ml (7.0 mmol) of styrene, 0.04 ml (0.28 mmol) divinylbenzene and 0.5 g (0.515 mmol) of O–B-EG600 (its CMC is about 0.15 mg ml^{-1}) were dispersed in 100 ml (5.56 mol) deionized water (the concentration is about 33.3 times the CMC). After stirring for 30 min, 0.04 g (0.24 mmol) AIBN was added in a N_2 atmosphere. The reaction mixture was stirred for 6 h at a temperature of 72 °C. Then the mixture containing the product was evaporated by rotary evaporatoration to eliminate any unreacted styrene, divinylbenzene and water, and P(St-*co*-O–B-EG600) CSNPs were obtained. P(St-*co*-O–B-EG1500), P(St-*co*-O–B-EG2000) and P(MMA-*co*-O–B-EG600) CSNPs were also prepared *via* the same route using O–B-EG1500 (CMC is about 0.43 mg ml^{-1}), O–B-EG2000 (CMC is about 0.52 mg ml^{-1}) and MMA as starting materials, respectively. The dosages of both O-B-EG1500 and O-B-EG2000 are 33.3 times than their CMCs.

P(St-co-O–B-EG600) colloisosomes: 0.05 g of P(St-*co*-O–B-EG600) CSNPs were dispersed in 50 ml (2.78 mol) deionized water. 1.0 ml of benzene was then added in the mixture. After stirring for 30 min at 41 °C, the system was quenched to 0 °C with an ice bath under a negative pressure (the negative pressure was applied by a vacuum) and stirring continued for another 30 min. Colloidosomes with tightly connected CSNPs were finally obtained. P(St-*co*-O–B-EG1500), P(St-*co*-O–B-EG2000) and P(MMA-*co*-O–B-EG600) colloidosomes were also prepared *via* the same using P(St-*co*-O–B-EG1500), P(St-*co*-O–B-EG2000) and P(MMA-*co*-O–B-EG600) CSNPs as starting materials.

2.3 Characterization

To obtain microscope images of the resultant products, samples in deionized water were deposited dropwise onto aluminium sheets. After air-drying for 10 h at room temperature, the samples were gold sputtering treated, and a field emission scanning electron microscope (FE-SEM, LEO-1530) was used to observe the surface morphology of the resulting products.

Transmission electron microscopy (TEM) measurements were performed with a JEM2100 at an acceleration voltage of 200 kV. To prepare the TEM samples, a small drop of the resultant product solution was deposited onto a carbon-coated copper electron microscopy (EM) grid and then dried under room temperature at atmospheric pressure.

An optical microscope was also used to observe the morphology of the colloidosomes. Samples in aqueous solution were deposited dropwise onto a microscope slide, and measured using a Metallurgical Microscope (ECLIPSE ME600L).

The particle size of the colloidosomes was characterized by dynamic light scattering (DLS) on a ZetaPALS. For the study of temperature-dependence of particle size, the diameter of the samples were measured by DLS at predetermined temperatures between 24 and 68 °C, and each temperature was maintained for at least 10 min.

To investigate the small molecule controlled release of the colloisosomes, pyrene in benzene solution (3.0 mmol L^{-1}) was used as template when preparing the colloidosomes. Consequently, fluorescence marked benzene was encapsulated in the interior of the colloidosoms. Fluorescence microscope images of the pyrene encapsulated colloidosomes were obtained from an inverted fluorescence microscope (LeicaDMLL). Samples in aqueous solution were deposited dropwise on a microscope slide and dried at room temperature before observation. The fluorescence emission spectra of pyrene in this system were measured by fluorescence spectrophotometry on HITACHI F-7000 at predetermined temperatures, and each temperature was maintained for at least 10 min. (stimulation slit width: 1 nm, emission slit width: 5 nm, scanning speed: 60 nm min^{-1}). The intensity of the emission peak at 373 nm (I_M) was calculated to elucidate the state of pyrene in the system as an effect of temperature.

3. Results and discussion

3.1 Structure

We chose an amphiphilic oligomer octadecyl, polyethylene glycol butenedioate (O–B-EG) with a hydrophobic chain and a hydrophilic chain linked on each side of the carbon–carbon double bond as the surfactant to synthesize CSNPs. The synthesis of O–B-EG has been demonstrated in our early work.[59] In aqueous solution, O–B-EG molecules readily form amphiphilic micelles. Hydrophobic monomers compatibilized in the cores of micelles can copolymerize with O–B-EG to form CSNPs. To form a highly cross-linked polymeric core, hydrophobic cross-linkers such as divinylbenzene and ethyleneglycol diacrylate were used when synthesizing CSNPs (these densely cross-linked cores can prevent the dissolution of CSNPs when preparing colloidosomes using oil as the template). Fig. 1A and its insert present the SEM image of P(St-*co*-O–B-EG600) CSNPs. These CSNPs exhibit relatively monodisperse particle size, with diameters in the range

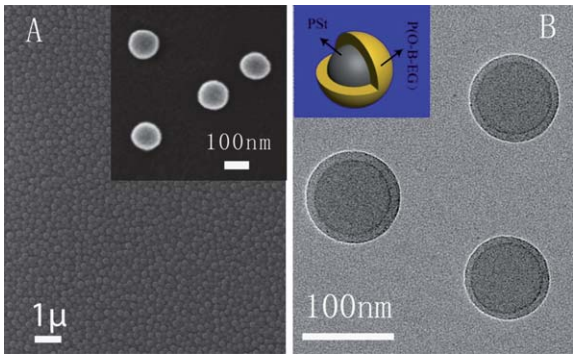

Fig. 1 (A) SEM, (B) TEM images of P(St-*co*-O–B-EG600) CSNPs, insert in (A) is the high resolution SEM image of P(St-*co*-O–B-EG600) CSNPs while insert in (B) is the model of the CSNPs.

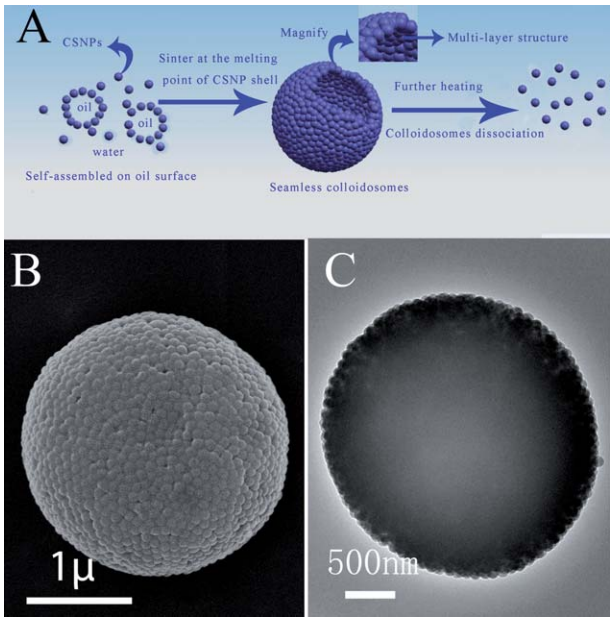

Fig. 2 (A) Structure, formation and dissociation mechanism of seamless colloidosomes; (B) SEM, (C) TEM images of seamless colloidosomes constructed from P(St-*co*-O–B-EG600) CSNPs.

of 100–110 nm. Clear core–shell structures are illustrated in Fig. 1B. The NPs have 80–90 nm diameter cores and 8–10 nm thick shells. ^{1}H NMR was used to confirm the components of these CSNPs. As cross-linked P(St-*co*-O–B-EG) NPs can not be dissolved, we synthesized non-cross-linked P(St-*co*-O–B-EG) NPs for component testing using ^{1}H NMR. Protons derived from both PSt and P(O–B-EG) can be observed in the ^{1}H NMR spectrum measureed in $CDCl_3$ (Fig. 2SA†), but only protons derived from PEG chains can be observed in the ^{1}H NMR spectrum measured in D_2O (Fig. 2SB†), indicating that the NPs exhibit PSt cores and P(O–B-EG) shells in aqueous solution (as shown in the insert of Fig. 1B).[60,61] Our previous work[59] has demonstrated that O–B-EG micelles were constructed from regularly arranged O–B-EG molecules which led to a high crystallinity. We also found that P(St-*co*-O–B-EG) CSNPs shells have excellent crystallinity. For example, P(St-*co*-O–B-EG600), P(St-*co*-O–B-EG1500) and P(St-*co*-O–B-EG2000) CSNPs synthesized using O–B-EG600, O–B-EG1500 and O–B-EG2000 as surfactants exhibit evident melting peaks at 41, 48 and 54 °C in DSC curves, respectively (Fig. 3S, ESI†). These low melting points are very important for the fabrication of our colloidosomes in aqueous solution.

The fabrication of our colloidosomes simply includes two steps (as shown in Fig. 2A). First, the oil to be encapsulated is emulsified in water containing CSNPs which are absorbed on the surface of oil droplets. Second, this system is heated to the temperatures which approximate to the melting points of the CSNP shells. After remaining at these temperatures for 30 min, the system was quenched to 0 °C and, colloidosomes constructed by the seamless connection of nanoparticles are obtained. In the second step, a negative pressure applied to the system is important to the formation of a seamlessly connecting structure during quenching. Under a negative pressure, the evaporation of the oil phase accelerates more quickly than that of the water phase. As a result, the colloidosomes shrink with the evaporation of oil, which facilitates the formation of tight surface structure. Figure 4S (ESI†) gives the images of CSNPs in aqueous solution and colloidosomes in aqueous solution. Clearly, after the formation of colloidosomes, the solution becomes milky and opaque which indicates the production of CSNPs aggregates with larger particle size. We also found that the colloidosome solution system has excellent stability. After standing for weeks, no precipitation or delamination was observed. This is attributed to the strong hydrophibility of the CSNP shells which are constructed from PEG segments, enhancing the interactions (for example: hydrogen bonds) between the colloidosomes and water.

Fig. 2B and C show the FE-SEM image and TEM image, respectively, of a colloidosome constructed from P(St-*co*-O–B-EG600) CSNPs. CSNPs are melted together, and the seams between the CSNPs are filled with polymer. Though the CSNPs are linked together randomly, the resultant colloidosomes exhibit a regular sphere-like structure. Here, the CSNP shell constructed from P(O–B-EG) plays an important role in the formation of this unique structure. First, P(O–B-EG) acts as a cross-linker for the bonding of the CSNPs, the melting P(O–B-EG) shells tangle together to fill the seams between CSNPs. Second, the low melting point of P(O–B-EG) makes it possible for the locking of CSNPs in aqueous solution. This advantage not only simplifies the stabilization of colloidosomes but also facilitates the encapsulation of target molecules. During our experimental process, we found that P(St-*co*-O–B-EG1500) and P(St-*co*-O–B-EG2000) CSNPs can form well-defined colloidosomes using the method presented above (Fig. 5S†). This method is also available for other hydrophobic acrylate monomer. For example, we have synthesized P(MMA-*co*-O–B-EG) CSNPs, and also obtained tightly bonded colloidosomes (Fig. 6S in ESI†). To elucidate the formation mechanism of this type of seamless colloidosomes, DLS was used to monitor the diameter change when synthesizing seamless colloidosomes. Figure 7S† gives the diameter distribution of P(St-*co*-O–B-EG600) CSNPs in the oil-in-water system before heating and after heating for 10 min and 20 min, respectively. The peak at around 120 nm is attributed to single CSNPs and peaks at diameters higher than 1000 nm are assigned to the colloidosomes. It is found that with the increase of heating time, the intensity of the peak at around 120 nm decreases

significantly, while the intensity of the peaks at diameters higher than 1000 nm evidently increase. Moreover, peaks attributed to the colloidosomes also move to higher diameter with the increase of heating time. These results indicate that partly the CSNPs self-assemble on the surface of the oil to form colloidosomes and partly that the CSNPs dissociate in the system before heating. However, when heating the system, dissociated CSNPs transfer to the surface of colloidosomes and interact with other CSNPs because the surface of the CSNPs are melted. Consequently, with the increase of heating time, colloidosomes with seamless and multi-layer structures grow gradually (as shown in Fig. 2A).

As this special self-assembly of CSNPs is guided by oil, the content of oil phase in aqueous solution may influence the morphology of colloidosomes. For example, when using benzene as template, 1–5 vol% would be appropriate for the formation of unique colloidosomes. A lower content results in a non-tightly bonding structure (Fig. 8S†), but a higher content leads to even more complicated structures. As shown in Fig. 3A, the coexistence of sphere-like structure, cylindrical structure and lamellar structure is clear. This is because a lower oil content results in smaller droplets which decreases the amount of CSNPs absorbed on the droplet surface and induces an unconsolidated aggregation. On the other hand, the emulsifying capacity of CSNPs is not strong. Oil can not be emulsified to form a spherical morphology but instead forms a lamellar structure if the oil content is too large. The TEM image of the lamellar structure (Fig. 3B) exhibits an interesting phenomenon that suggests the lamellar structure could be dilacerated like a piece of paper, without any dissociation of CSNPs. This result gives sufficient proof that the lamellar structures, as well as the colloidosomes, are constructed by tightly connected NPs and have excellent mechanical strength. We also found that the dosage of CSNPs exhibits an evident influence on the morphology of this type of colloidosomes. 0.03–0.1 g of CSNPs is suitable for preparing spherical seamless colloidosomes when the content of benzene is kept at 2.0 vol%. Lower and higher doses of CSNPs result in incompact and nonspherical structures, respectively (see Fig. 9S in ESI†).

Although no seam exists on the surface of the colloidosomes because it is constructed by tightly bonded NPs, hollow structures are still located in interior of the colloidosomes. Fig. 4A and B give an example of the hollow structure. These two images emphasize a colloidosome with surface on which a hole defect can be observed clearly. By looking into the colloidosome through the deep hole, a hollow structure is obvious. The deep hole also indicates that the colloidosomes are constructed by multilayers and not a monolayer of NPs. This multilayer NP morphology is helpful for both the supporting of hollow structure and the formation of an airtight solid shell. The morphology of these colloidosomes has also been observed by optical microscope. Fig. 4C and D show the normal picture and polarized light picture of the P(St-*co*-O–B-EG600) colloidosomes in aqueous solution, respectively. Sphere-like structures are suspended in the solution and, the polarizing image gives an intuitive view of hollow structures with an optical ring covering on each sphere. This is because only ordered structures can be observed in a polarizing picture. So the optical ring is attributed to the solid shell composed of P(St-*co*-O–B-EG600) CSNPs, while the dark core is the result of the hollow structure. The crystallization of P(O–B-EG600), facilitated our observation of the microstructure of the colloidosomes in aqueous solution.

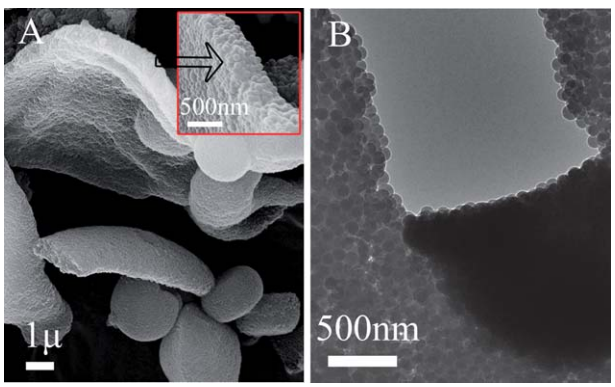

Fig. 3 (A) SEM image of colloidosomes self-assembled in a 10 vol% benzene–water system and (B) TEM image of lamellar structure (these structures are constructed from P(St-*co*-O–B-EG600) core–shell structured CSNPs).

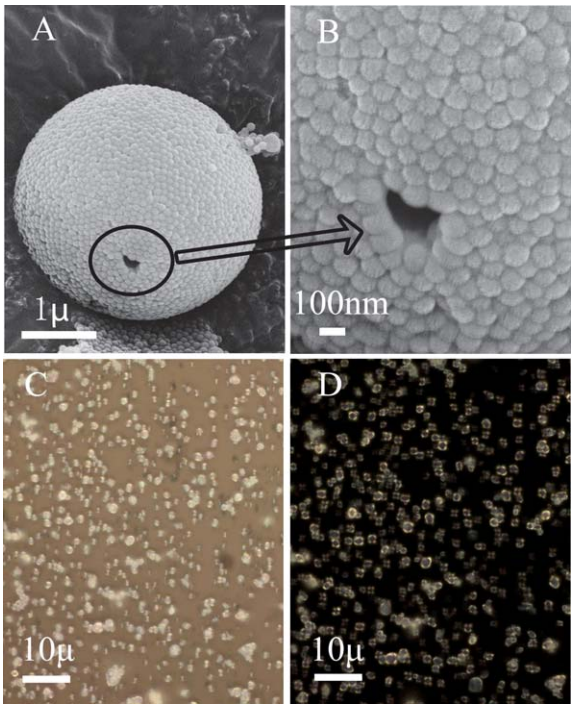

Fig. 4 SEM image (A) and high resolution SEM image (B) of colloidosome with a hole; (C) normal optical picture and (D) polarizing optical picture of colloidosomes in aqueous solution (these structures are constructed from P(St-*co*-O–B-EG600) CSNPs).

3.2 Reversible self-assembly behavior

This self-assembly of NPs shows excellent reversibility. The resultant colloidosomes in aqueous solution dissociate into NPs when the system is heated. For example, we have used dynamic light scattering (DLS) to test the temperature dependence of the diameter of colloidosomes. As shown in Fig. 5A, colloidosomes constructed from P(St-*co*-O–B-EG600), P(St-*co*-O–B-EG1500) and P(St-*co*-O–B-EG2000) CSNPs exhibit an abrupt change of

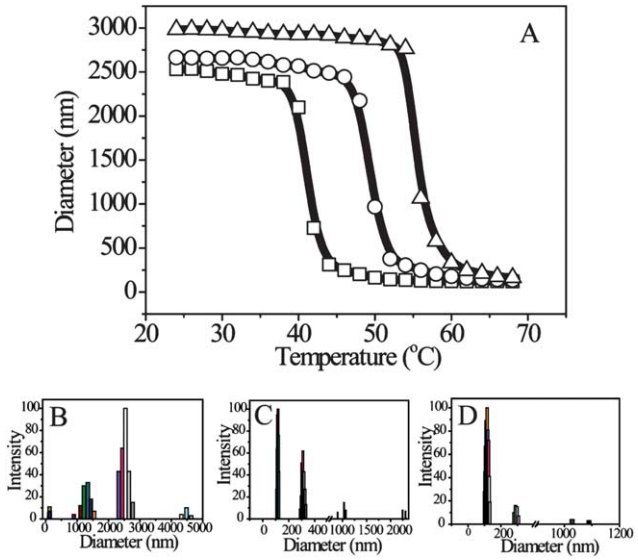

Fig. 5 (A) Particle sizes of colloidosomes in aqueous solution as an effect of temperature: (□) P(St-*co*-O–B-EG600) CSNP colloidosomes, (○) P(St-*co*-O–B-EG1500) CSNP colloidosomes, (△) and P(St-*co*-O–B-EG2000) CSNP colloidosomes; Size distribution of P(St-*co*-O–B-EG600) CSNP colloidosomes at 30 (B), 44 (C) and 60 °C (D).

diameter at the temperatures around 43 °C, 50 °C and 56 °C, respectively. These temperatures are about 2 °C higher that the melting points of the P(O–B-EG)s. The diameters of these three systems measured by DLS finally equilibrated at around 120 nm, 134 nm and 152 nm, respectively, which are approximate to the diameters of the non-aggregated nanoparticles. This result suggests that our colloidosomes can easily dissociate into individual CSNPs at high temperatures. The particle size distribution of P(St-*co*-O–B-EG600) based colloidosomes at temperatures of 30, 44 and 60 °C are shown in Fig. 5B, C and D, respectively. Obviously, with the increase of temperature, the content of particles with larger size decreases but the content of particles with smaller size increases, indicating that the colloidosomes did not dissociate into single CSNPs completely in one-step. So, it can be speculated that the dissociation of colloidosomes at high temperature is a gradual process but not a one-step procedure. Moreover, if the oil such as *n*-hexane or benzene is again added to the system with dissociated CSNPs at the temperature of the P(O–B-EG) melting point, and then the system is treated with the same conditions that we first used to prepare the colloidosomes, tightly bonded colloidosomes can still be obtained. So, by simply controlling the temperature, the colloidosomes can form and dissociate reversibly.

For CSNPs, the melting point of the P(O–B-EG) shell is much lower than the boiling point of water. When heating the system to the melting point of P(O–B-EG), the shells of the NPs become flexible with high viscosity. Under the shape direction of an oil droplet, CSNPs aggregate on the surface of the oil and interact with each other by the fusing together of the P(O–B-EG) shells. Then a quenching treatment freezes the nanoparticle shells, and results in the colloidosome structure. However, when heating colloidosome aqueous solutions to 2 °C higher than the P(O–B-EG)s melting point, the melted P(O–B-EG) shells exhibit low viscosity. The interaction between NPs resulted from the low viscosity is so weak that it can not support the colloidosome structure. Therefore, the colloidosomes easily dissociate into individual CSNPs (as shown in Fig. 2A). By changing the molecular weight of PEG, we obtained a series of colloidosomes with different dissociation temperatures ranging from 43 to 56 °C. This is very important for a molecule encapsulation and controlled release system.

3.3 Small molecule encapsulation and release

To evaluate the small molecule encapsulating properties, benzene fluorescent marked with 3.0 mmol L^{-1} of pyrene was used as an oil template when fabricating our colloidosomes. So pyrene dissolved in benzene was encapsulated in the hollow colloidosomes. The fluorescence microscope image shown in Fig. 6A gives an observation which indicates the presence of pyrene benzene solution encapsulated colloisosomes. Obvious blue light spots on the black–white underlay imply an efficient encapsulation of hydrophobic small molecules. We then measured the fluorescence emission spectra of pyrene in this system at different temperatures (the results are shown in Fig. 10S†). In the fluorescence emission spectra, the peak at 373 nm is from a single pyrene molecule whose intensity greatly depends on the polarity of surrounding solvent.[62] A stronger polarity leads to a higher intensity, while a weaker polarity induces a lower intensity. Consequently, the change in the peak intensity at 373 nm (I_M) in the fluorescence emission spectra reflects the variation in status of pyrene in the system. Fig. 6B illustrates the effect of temperature on the intensity of the peak at 373 nm in the fluorescence emission spectra of pyrene encapsulated in colloidosomes made from P(St-*co*-O–B-EG600), P(St-*co*-O–B-EG1500) and P(St-*co*-O–B-EG2000) CSNPs. These three curves exhibit almost the same changing process. I_M firstly decreases slightly with increasing temperature and then increases significantly around the colloidosome dissociation temperatures (for example: P(St-*co*-O–B-EG600) colloidosomes at 43 °C, P(St-*co*-O–B-EG1500) colloidosomes at 50 °C, P(St-*co*-O–B-EG2000) colloidosomes at 56 °C). However, a further increase of temperature results in a rapid decrease of I_M. It is a common view that fluorescence intensity of pyrene weakens with the increase of environmental temperature (this is also proved by the results shown in Fig. 11S in ESI†), which accords well with our results at low temperatures.

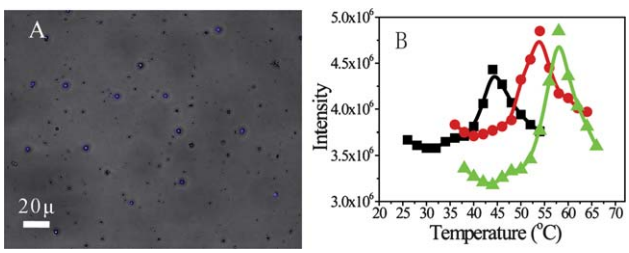

Fig. 6 Fluorescence microscope image of colloidosomes encapsulated pyrene benzene solution (A); influence of temperature on intensity of I_M (peak at 373 nm) in the fluorescence emission spectra of pyrene (B), P(St-*co*-O–B-EG600) colloidosomes (■), P(St-*co*-O–B-EG1500) colloidosomes (●) and P(St-*co*-O–B-EG2000) colloidosomes (▲).

That an abnormal increase of I_M appears at the dissociation temperatures of colloidosomes implies a status change of the pyrene in the system. The temperature is higher than the melting points of the NPs shells, and the resulting colloidosomes dissociation into single NPs. Benzene with dissolved pyrene transmit into the water phase from the interior cores of the colloidosomes. Because the polarity of water is much higher than that of the NPs surface composed of PEG segments, I_M in the fluorescence emission spectra evidently increases. Furthermore, Fig. 6B also shows a rapid intensity decrease of I_M as the temperature further increases. This is because when the temperature is too high, the colloidosomes are dissociated completely. As a result, benzene with dissolved pyrene is dispersed in the water phase and form hydrophobic droplets. With the growth of hydrophobic droplets, the polarity of the environment which surrounds the pyrene decreases significantly, and I_M in the fluorescence emission spectra decrease accordingly. On the other hand, the higher temperature acts as another driving force that promotes the decrease of I_M. This evidence not only gives proof for the dissociation of colloidosomes at high temperatures but also reveals that our colloidosomes have a potential application in drug encapsulation and controlled release. Hydrophobic drugs can be encapsulated in the hollow structure of the colloidosomes and released when the temperature is higher than the colloidosomes dissociation temperature. Furthermore, when decreasing the temperature, we found that the intensity change of I_M (as shown in Figure 11Sd in ESI†) is almost the inverse process of the one when increasing the temperature (see in Fig. 6B), which indicates that pyrene in benzene droplets could be reversibly encapsulated in the colloidosomes. Consequently, it is reasonable to consider that our colloidosomes can reversibly encapsulate and release hydrophobic molecules.

4. Conclusions

In summary, we have introduced a novel method to stabilize colloidosomes self-assembled from CSNPs on liquid–liquid interface in an oil–water system. These CSNPs are constructed of cross-linked polymer cores and amphiphilic shells with melting points which much lower than the boiling point of water. By simply heating and quenching the oil–water system, a seamless connection between nanoparticles could be realized. This new type of colloidosome would dissociate into single CSNPs when the system is heated up to 2 °C higher than the melting points of the CSNP shells. More importantly, by changing the molecular weight of PEG in the amphiphilic shells of the CSNPs, a series of colloidosomes with different dissociation temperatures ranging from 43 to 56 °C can be obtained. These colloidosomes have excellent controlled release properties of hydrophobic molecules. Target molecules are encapsulated in the hollow cores of the colloidosomes at low temperatures, but released rapidly when the temperature rises to the dissociation temperatures of the colloidosomes. We believe that the seamless structure and controllable dissociation temperature of this new type of colloidosomes may prove to be useful in the application of drug controlled release. Moreover, this simple and effective method for the stabilization of colloidosomes may also be interesting for the production of polymeric aggregations in oil–water systems.

Acknowledgements

This work was supported by the National Natural Science Foundation of China (50873082, 30700020); Research Fund for the Doctoral Program of Higher Education (20070384047); Scientific and Technical Project of Fujian Province of China (2009J1009, 2010H6021, 2010J01306).

References

1 Y. N. Xia, Y. D. B.GatesYin and Y. Lu, *Adv. Mater.*, 2000, **12**, 693.
2 W. H. Binder, *Angew. Chem., Int. Ed.*, 2005, **44**, 5172.
3 C. M. Soukoulis, *Photonic Band Gap Materials*, Kluwer Academic Publishers, Dordrecht, 1996.
4 P. L. Flaugh, S. E. O'Donnell and S. A. Asher, *Appl. Spectrosc.*, 1984, **38**, 847.
5 I. M. Krieger and F. M. O'Neill, *J. Am. Chem. Soc.*, 1968, **90**, 3114.
6 P. A. Hiltner and I. M. Krieger, *J. Phys. Chem.*, 1969, **73**, 2386.
7 J. W. Goodwin, R. H. Ottewill and A. Parentich, *J. Phys. Chem.*, 1980, **84**, 1580.
8 J. M. Weissman, H. B. Sunkara, A. S. Tse and S. A. Asher, *Science*, 1996, **274**, 959.
9 G. Pan, R. Kesavamoorthy and S. A. Asher, *Phys. Rev. Lett.*, 1997, **78**, 3860.
10 G. Pan, R. Kesavamoorthy and S. A. Asher, *J. Am. Chem. Soc.*, 1998, **120**, 6525.
11 J. H. Holtz and S. A. Asher, *Nature*, 1997, **389**, 829.
12 J. H. Holtz, J. W. Holtz, C. H. Munro and S. A. Asher, *Anal. Chem.*, 1998, **70**, 780.
13 C. López, *Adv. Mater.*, 2003, **15**, 1679.
14 S. H. Park and Y. Xia, *Chem. Mater.*, 1998, **10**, 1745.
15 S. H. Park and Y. Xia, *Adv. Mater.*, 1998, **10**, 1045.
16 B. Gates, Y. Yin and Y. Xia, *Chem. Mater.*, 1999, **11**, 2827.
17 Z. Y. Zhong, Y. D. Yin, B. Gates and Y. N. Xia, *Adv. Mater.*, 2000, **12**, 206.
18 D. K. Yi and D. Y. Kim, *Chem. Commun.*, 2003, 982.
19 H. W. Deckman and J. H. Dunsmuir, *Appl. Phys. Lett.*, 1982, **41**, 377.
20 C. B. Roxlo, H. W. Deckman and B. Abeles, *Phys. Rev. Lett.*, 1986, **57**, 2462.
21 Y. C. Fisher and H. P. Zingsheim, *J. Vac. Sci. Technol.*, 1981, **19**, 881.
22 J. C. Hulteen, D. A. Treichel, M. T. Smith, M. L. Duval, T. R. Jensen and R. P. V. Duyne, *J. Phys. Chem. B*, 1999, **103**, 3854.
23 S. Nishimura, N. Abrams, B. A. Lewis, L. I. Halaoui, T. E. Mallouk, K. D. Benkstein, J. van de. Lagemaat and A. J. Frank, *J. Am. Chem. Soc.*, 2003, **125**, 6306.
24 G. I. N. Waterhouse and M. R. Waterland, *Polyhedron*, 2007, **26**, 356.
25 R. Mayoral, J. Requena, J. S. Moya, C. López, A. Cintas, H. Miguez, F. Meseguer, L. Vázquez, M. Holgado and á. Blanco, *Adv. Mater.*, 1997, **9**, 257.
26 H. Miguez, F. Meseguer, C. López, A. Blanco, J. S. Moya, J. Requena, A. Mifsud and V. Fornes, *Adv. Mater.*, 1998, **10**, 480.
27 N. D. Denkov, O. D. Velev, P. A. Kralchevsky, I. B. Ivanov, J. H. Yoshimura and K. Nagayamat, *Langmuir*, 1992, **8**, 3183.
28 Y. H. Ye, F. LeBlanc, A. Hache and V. V. Truong, *Appl. Phys. Lett.*, 2001, **78**, 52.
29 P. Jiang, J. F. Bertone, K. S. Hwang and V. L. Colvin, *Chem. Mater.*, 1999, **11**, 2132.
30 Y. F. Liu, S. P. Wang, J. W. Lee and N. A. Kotov, *Chem. Mater.*, 2005, **17**, 4918.
31 S. H. Park and Y. Xia, *Langmuir*, 1999, **15**, 266.
32 J. G. Deng, X. M. Tao, P. Li, P. Xue, Y. H. Zhang, X. H. Sun and K. C. Kwan, *J. Colloid Interface Sci.*, 2005, **286**, 573.
33 C. T. Kresge, M. E. Leonowicz, W. J. Roth, J. C. Vartuli and J. S. Beck, *Nature*, 1992, **359**, 710.
34 D. D. Archibald and S. Mann, *Nature*, 1993, **364**, 430.
35 P. Behrens and G. D. Stucky, *Angew. Chem., Int. Ed. Engl.*, 1993, **32**, 696.
36 H. Yang, N. Coombs and G. A. Ozin, *Nature*, 1997, **386**, 692.
37 O. D. Velev, T. A. Jede, R. F. Lobo and A. M. Lenhoff, *Chem. Mater.*, 1998, **10**, 3597.
38 B. T. Holland, C. F. Blanford and A. Stein, *Science*, 1998, **281**, 538.
39 B. T. Holland, C. F. Blanford, T. Do and A. Stein, *Chem. Mater.*, 1999, **11**, 795.

40 S. Reculusa and S. Ravaine, *Appl. Surf. Sci.*, 2005, **246**, 409.
41 A. D. Dinsmore, M. F. Hsu, M. G. Nikolaides, M. Marquez, A. R. Bausch and D. A. Weitz, *Science*, 2002, **298**, 1006.
42 Y. Lin, H. Skaff, T. Emrick, A. D. Dinsmore and T. P. Russell, *Science*, 2003, **299**, 226.
43 W. H. Binder, *Angew. Chem., Int. Ed.*, 2005, **44**, 5172.
44 L. Hong, S. Jiang and S. Granick, *Langmuir*, 2006, **22**, 9495.
45 B. S. Kim and T. A. Taton, *Langmuir*, 2007, **23**, 2198.
46 K. H. Roh, M. Yoshida and J. Lahann, *Langmuir*, 2007, **23**, 5683.
47 C. E. Snyder, A. M. Yake, J. D. Feick and D. Velegol, *Langmuir*, 2005, **21**, 4813.
48 B. Sun, Y. Zhang, K. J. Gu, Q. D. Shen, Y. Yang and H. Song, *Langmuir*, 2009, **25**, 5969.
49 J. J. Teo, Y. Chang and H. C. Zeng, *Langmuir*, 2006, **22**, 7369.
50 Y. Pan, J. Gao, B. Zhang, X. Zhang and B. Xu, *Langmuir*, 2009, **26**, 4184.
51 B. P. Binks and T. S. Horozov, in *Colloidal Particles at Liquid Interfaces* (eds: B. P. Binks, T. S. Horozov), Cambridge University Press, Cambridge, UK 2006, Ch. 1.
52 B. P. Binks and R. Murakami, *Nat. Mater.*, 2006, **5**, 865.
53 B. P. Binks, B. Duncumb and R. Murakami, *Langmuir*, 2007, **23**, 9143.
54 E. M. Herzig, K. A. White, A. B. Schofield, W. C. K. Poon and P. S. Clegg, *Nat. Mater.*, 2007, **6**, 966.
55 R. Murakami and A. Bismarck, *Adv. Funct. Mater.*, 2010, **20**, 732.
56 H. W. Gu, Z. M. Yang, J. H. Gao, C. K. Chang and B. Xu, *J. Am. Chem. Soc.*, 2005, **127**, 34.
57 B. P. Binks and S. O. Lumsdon, *Langmuir*, 2000, **16**, 8622.
58 B. Binks and J. H. Clint, *Langmuir*, 2002, **18**, 1270.
59 C. H. Yuan, Y. T. Xu, Y. M. Deng, J. F. Chen, Y. L. Liu and L. Z. Dai, *Soft Matter*, 2009, **5**, 4642.
60 H. S. Peng, D. Y. Chen and M. Jiang, *Langmuir*, 2003, **19**, 10989.
61 X. M. Yao, D. Y. Chen and M. Jiang, *Macromolecules*, 2004, **37**, 4211.
62 F. M. Winnik, *Macromolecules*, 1990, **23**, 233.

